Published OnlineFirst May 10, 2018; DOI: 10.1158/0008-5472.CAN-17-3014

Molecular Cell Biology

Cancer Research

miR-590-3p Promotes Ovarian Cancer Growth and Metastasis via a Novel FOXA2–Versican Pathway

Mohamed Salem[1], Jacob A. O'Brien[1], Stefanie Bernaudo[1], Heba Shawer[2], Gang Ye[1], Jelena Brkić[1], Asma Amleh[2], Barbara C. Vanderhyden[3], Basel Refky[4], Burton B. Yang[5], Sergey N. Krylov[6,7], and Chun Peng[1,7]

Abstract

miRNAs play important roles in gene regulation, and their dysregulation is associated with many diseases, including epithelial ovarian cancer (EOC). In this study, we determined the expression and function of miR-590-3p in EOC. miR-590-3p levels were higher in high-grade carcinoma when compared with low-grade or tumors with low malignant potential. Interestingly, plasma levels of miR-590-3p were significantly higher in patients with EOC than in subjects with benign gynecologic disorders. Transient transfection of miR-590-3p mimics or stable transfection of mir-590 increased cell proliferation, migration, and invasion. *In vivo* studies revealed that mir-590 accelerated tumor growth and metastasis. Using a cDNA microarray, we identified forkhead box A2 (FOXA2) and versican (VCAN) as top downregulated and upregulated genes by mir-590, respectively. miR-590-3p targeted FOXA2 3′ UTR to suppress its expression. In addition, knockdown or knockout of FOXA2 enhanced cell proliferation, migration, and invasion. Overexpression of FOXA2 decreased, whereas knockout of FOXA2 increased VCAN mRNA and protein levels, which was due to direct binding and regulation of the VCAN gene by FOXA2. Interrogation of the TCGA ovarian cancer database revealed a negative relationship between FOXA2 and VCAN mRNA levels in EOC tumors, and high FOXA2/low VCAN mRNA levels in tumors positively correlated with patient survival. Finally, overexpression of FOXA2 or silencing of VCAN reversed the effects of mir-590. These findings demonstrate that miR-590-3p promotes EOC development via a novel FOXA2–VCAN pathway.

Significance: Low FOXA2/high VCAN levels mediate the tumor-promoting effects of miR-590-3p and negatively correlate with ovarian cancer survival. *Cancer Res; 78(15); 4175–90. ©2018 AACR.*

Introduction

Epithelial ovarian cancer (EOC) is the most common form of ovarian cancer and has the highest mortality rate among all gynecologic malignancies (1). There are no effective early screening methods for EOC; thus, most cases are not detected until late stages when the cancer has spread to other organs. Ovarian cancer cells detached from primary tumors often settle on the peritoneum and omentum, as well as adjacent organs (2). However, tumor cells have also been detected in the blood of patients with ovarian cancer, suggesting an additional hematogenous path by which cancer cells invade through blood and lymph vessels to establish secondary tumors (3).

miRNAs are small noncoding RNAs that regulate gene expression primarily at the posttranscriptional levels. miRNA genes are transcribed into primary miRNAs, processed into precursor (pre)-miRNAs, and exported from the nucleus. Within the cytoplasm, pre-miRNAs are further processed into mature miRNAs (4). It is well accepted that miRNAs play critical roles in many developmental and physiologic events. Moreover, aberrant miRNA expression has been implicated in the pathogenesis of human diseases, including cancer (4).

miR-590-3p is contained within an intron of the eukaryotic translation initiation factor 4H gene. miR-590-3p was first reported to enhance cardiomyocyte proliferation and cardiac regeneration after myocardial infarction (5). More recently, the effects of miR-590-3p on several types of cancer have been reported (6–8). Although the role of miR-590-3p in ovarian cancer is unknown, an RNA sequencing (RNA-seq) study has identified miR-590-3p as one of the miRNAs dysregulated in EOC tumors (9), suggesting its potential role in EOC development.

Forkhead box A2 (FOXA2) is a transcription factor involved in the regulation of embryo development, as well as metabolism and homeostasis (10). Recent studies suggest that FOXA2 also plays a role in cancer development. Tumor-suppressive effects of FOXA2 have been reported in pancreatic cancer (11), lung cancer (12, 13), and gastric cancer (14). In breast cancer,

[1]Department of Biology, York University, Toronto, Canada. [2]Department of Biology, American University in Cairo, New Cairo, Egypt. [3]Department of Cellular and Molecular Medicine, University of Ottawa, Ottawa, Canada. [4]Department of Surgical Oncology, Mansoura Oncology Center, Mansoura, Egypt. [5]Sunnybrook Research Institute and Department of Laboratory Medicine and Pathobiology, University of Toronto, Toronto, Canada. [6]Department of Chemistry, York University, Toronto, Canada. [7]Centre for Research on Molecular Interactions, York University, Toronto, Canada.

Note: Supplementary data for this article are available at Cancer Research Online (http://cancerres.aacrjournals.org/).

Corresponding Author: Chun Peng, Department of Biology, York University, 4700 Keele St, Toronto, Ontario M3J 1P3, Canada. Phone: 416-736-2100; Fax: 416-736-5698; E-mail: cpeng@yorku.ca

doi: 10.1158/0008-5472.CAN-17-3014

Published OnlineFirst May 10, 2018; DOI: 10.1158/0008-5472.CAN-17-3014

both tumor-suppressing (15) and tumor-promoting effects (16) have been found. Interestingly, the role of FOXA2 in liver cancer development is sexually dimorphic, with tumor-suppressive effects in females and tumor-promoting effects in males (17).

Versican (VCAN) is a large proteoglycan and a major component of the extracellular matrix. Numerous studies have shown that VCAN is frequently overexpressed in tumor tissues and promotes processes associated with tumor development, such as adhesion, proliferation, migration, invasion, and angiogenesis (18). In advanced stage serous ovarian cancer, high VCAN expression in the tumor stroma is associated with shorter survival (19), and *in vitro* studies suggest that VCAN promotes ovarian cancer cell invasion (20).

The aim of this study was to investigate the role of miR-590-3p in ovarian cancer development. Herein, we report that miR-590-3p is upregulated in tumor tissues and plasma samples of patients with EOC and exerts tumor-promoting effects. We further demonstrate that FOXA2 is a direct target of miR-590-3p and identify FOXA2 as a negative regulator of VCAN. Finally, we show that lower FOXA2 and higher VCAN levels in the same tumors are significantly associated with decreased survival rates in patients with ovarian cancer.

Materials and Methods

Patient specimen

Two sets of samples were used in this study. The first set, which contained tissues and plasma samples, was collected at Mansoura Oncology Center in Egypt (Supplementary Table S1A) with approval by the Institutional Review Board of the American University in Cairo. The other set of tumor samples was obtained from the Ottawa Ovarian Cancer Tissue Bank (Supplementary Table S1B) through a protocol approved by the Research Ethics Board of The Ottawa Hospital (Ottawa, Canada). For the first set of samples, control ovarian tissues were taken from women who underwent hysterectomy and/or oophorectomy for benign gynecologic conditions. Blood samples were collected prior to surgery. All patients provided written informed consent. The studies were conducted in accordance with the ethical guidelines of Canadian Tri-Council and U.S. Common Rule.

Cell culture and transient transfection

EOC cell lines, ES-2, SKOV3.ip1, and HEY, were obtained and cultured, as reported previously (21). The SKOV3.ip1 was transfected with a luciferase plasmid (pMIR-REPORT, Ambion) to allow for bioluminescent imaging. OVCAR3 was purchased from ATCC and cultured in RPMI1640 media (HyClone) supplemented with 20% FBS and 0.01 mg/mL insulin. All cell lines have been authenticated using short tandem repeat profile (IDEXX BioResearch). Cells were routinely tested to ensure they were free of *Mycoplasma* contamination using Mycoplasma Detection Kit-QuickTest (BioMake) and DAPI staining. Transient transfection of plasmids (0.25–1.5 μg), miRNA mimics, inhibitors, or siRNAs (150–200 nmol/L) was carried out in 6-well plates using Lipofectamine 2000 or Lipofectamine RNAiMAX (Life Technologies) following the manufacturer's suggested protocols. siRNAs, nontargeting negative control (NC), and miR-590-3p/5p mimic were purchased from GenePharma Co. Anti–miR-590-3p/5p and its corresponding NC were purchased from RiboBio. Their sequences are listed in Supplementary Table S2. The FOXA2 expression plasmid was purchased from GenScript.

Generation of mir-590 stable cell lines

A fragment containing hsa-mir-590 stem-loop sequence was generated using specific primers (Supplementary Table S2). PCR was carried out using Phusion DNA Polymerase, and the resulting product was cloned into the pRNAT-CMV3.2/Hygro Expression Vector (GenScript). Positive clones were selected using PCR and validated by sequencing. The clone with the correct sequence was subsequently transfected into ES-2, SKOV3.ip1, and HEY cells. To generate control cells, the same cell lines were transfected with pRNAT-CMV3.2/Hygro, without the mir-590 insert. Following transfection, cells were cultured with hygromycin (0.6 mg/mL for SKOV3.ip1 and HEY cells and 0.8 mg/mL for ES-2) to select mir-590–positive cells.

RNA extraction, reverse transcription, and real-time PCR

Total RNA was extracted from cells or tissues using TRIzol reagent (Invitrogen) and reverse transcribed into cDNA, as described previously (22). qRT-PCR was carried out using EvaGreen qPCR Master Mix (ABM), following the manufacturer's suggested protocol. The levels of mRNAs were normalized to GAPDH. Primer sequences are listed in Supplementary Table S2.

To measure miR-590-3p and miR-590-5p levels, small RNA–enriched total RNA was extracted using TRIzol reagent (Invitrogen) as reported previously (22, 23). The miR-590 levels in cells and tissues were measured using TaqMan PCR Kit (Thermo Fisher Scientific) and normalized to U6 snRNA. RNA was extracted from plasma samples using Qiagen miRNeasy Serum/Plasma Kit. A synthetic *C. elegans* cel-miR-39 miRNA mimic spike-in was used as an internal control. Relative quantification of mRNAs and miRNAs were calculated using the $2^{-\Delta\Delta C_t}$ method.

Migration, invasion, and proliferation assays

Transwell migration and invasion assays were performed as described previously (21) with the modification that migrated and invaded cell numbers were counted using an automated quantification plugin for ImageJ (24). Cell proliferation assays were conducted using manual cell counting or a real-time live-cell imaging system IncuCyte S3 (Essen Bioscience). Briefly, transfected cells were detached using Accutase (Corning) and seeded into a 96-well plate at the density of 2.5×10^3 cells/well. Four hours after seeding, images were taken every 4 hours for 68 hours.

Clonogenic assay

A total of 500 cells, stably overexpressing either mir-590 or its empty vector (EV), were seeded in a 6-well plate. After 15 to 20 days, colonies were fixed with 3.7% paraformaldehyde for 5 minutes, and stained with 0.05% crystal violet for 30 minutes. Plates were then washed, and the number of visible colonies were counted.

Microarray analysis

Total RNA was extracted from the ES-2 cell line overexpressing mir-590 and its EV-transfected control cell line ($n = 3$ wells). The cDNA microarray and subsequent analyses were conducted by the Princess Margaret Genomics Centre, Toronto, Canada (https://www.pmgenomics.ca/pmgenomics/). Hybridization was carried out using the Human HT-12 V4 BeadChip and data were imported in GeneSpring (v13.0) for analysis.

Published OnlineFirst May 10, 2018; DOI: 10.1158/0008-5472.CAN-17-3014

The data were first normalized using a standard (for Illumina arrays) quantile normalization followed by a "per probe" median centered normalization. Data were then filtered to remove the confounding effect probes that show no signal may have on subsequent analysis. Only probes that were above the 20th percentile of the distribution of intensities in 100% of any of the 1 of 2 groups were allowed to pass through this filtering. The final set contained 38,146 probes. A one-way ANOVA with a Benjamini–Hochberg false discovery rate–corrected $P < 0.05$ showed 4,259 significantly varying probes. A *post hoc* Tukey HSD test was used after the ANOVA and resulted in 2,483 significant probes. The microarray dataset has been deposited to the Gene Expression Omnibus repository under the accession number GSE113440.

Genes that showed a difference between the EV and mir-590 groups by 2.0-fold or more were organized into a heatmap using the Multi Experiment Viewer (MeV) Microarray Software Suite. The Cancer Genome Atlas (TCGA) ovarian cancer dataset in Oncomine (www.oncomine.org) was interrogated to determine whether these genes are dysregulated in EOC.

Protein extraction and immunoblotting

Cell lysates were prepared as described previously (21). To detect FOXA2, proteins were separated by 10% SDS-PAGE gels, then transferred to PVDF (Immobilon-P, Millipore Corp.) membranes for 1 hour. To resolve VCAN samples and GAPDH on the same gel, samples were loaded into 4% to 15% gradient gels and transferred to PVDF membranes for 14 hours using 40 volts in a cold room at 4°C. Membranes were blocked in 5% blocking buffer (5% skim milk in Tris-buffered saline and Tween-20) for 1 hour at room temperature and then incubated overnight with primary antibody at 4°C. Membranes were subsequently probed using horseradish peroxidase–conjugated secondary antibody (1:5,000) at room temperature for 2 hours. Protein signals were visualized using Luminata Classico Western HRP Substrate (EMD Millipore Corp.). FOXA2 antibody was obtained from Cell Signaling Technology (dilution 1:1,000), VCAN antibody was obtained from Boster (1:1,000), and GAPDH antibody was purchased from Santa Cruz Biotechnology (1:10,000).

Chromatin immunoprecipitation assay

Chromatin immunoprecipitation (ChIP) assays were conducted as reported previously (25). Briefly, cells were cross-linked and cell lysates were sonicated and precleared with Pierce Protein A/G Magnetic Beads (Thermo Fisher Scientific) for 1 hour at 4°C. The samples were incubated with fresh magnetic beads conjugated with either FOXA2 antibody or control IgG (Cell Signaling Technology) overnight at 4°C. DNA was extracted from the precipitated samples using the phenol–chloroform method. To design primers for VCAN, the *VCAN* gene was analyzed for consensus FOXA2-binding sites, 5′-[AC]A[AT]T[AG]TT[GT][AG][CT]T[CT]-3′, obtained from UniProt (26) using a program developed by us (source code available from http://peng.lab.yorku.ca/bioinformatics-tools). The *VCAN* promoter region was predicted using transcription start site–proximal TF-binding sites, promoter-associated histone markers (H3K4Me3 and H3K27Ac), and DNase hypersensitivity sites from the UCSC Genome Browser (27). Three sets of primers were designed to target: (i) a predicted FOXA2 binding site on the promoter; (ii) an intragenic site with two proximal predicted FOXA2-binding sites overlapping an open chromatin region with regulatory potential; and (iii) an intragenic site that overlaps an open chromatin region with no predicted FOXA2-binding sites, which serves as a negative control.

Luciferase assay

A fragment of FOXA2 3′ UTR, containing the predicted miR-590-3p–binding site, was generated by PCR using specific primers (Supplementary Table S2). The resulting PCR amplicon was cloned into pMIR-REPORT, downstream of the luciferase coding sequence. Cells were seeded in 12-well plates at a density of 7.5×10^4 cells/well, transfected with the FOXA2 3′ UTR construct, together with miR-590-3p mimics or its NC. At 24 hours after transfection, luciferase activity was measured using the Dual Luciferase Reporter Assay System (Promega) according to the manufacturer's instructions, as reported previously (23).

Tumor xenograft assays

The use of animals for this study was approved by York University Animal Care Committee. Five to 6-week-old female CD-1 nude mice were purchased from Charles River Laboratories and were housed under sterile conditions in Microisolator cages, fed standard chow diet with water, and maintained in a 12-hour light/dark cycle. To study tumor formation, mice were injected subcutaneously with 1.5×10^6 control or mir-590 stable ES-2 cells suspended in 150 μL PBS. Tumor size was measured every 2 days throughout the course of the experiment. The endpoint of the study was determined when tumor size reached 17 mm or if the animal showed any sign of sicknesses such as hunched posture, inactivity, hypothermia, or ulceration at the tumor site. To study tumor metastasis, two experiments were performed. In the first experiment, mice were injected intraperitoneally with 1×10^6 SKOV3.ip1 cells expressing EV or mir-590, suspended in 200 μL of PBS. Animals were monitored daily and the experiment was terminated at day 70 when some of the mice showed excessive abdominal distension or moribund. Mice were anaesthetized using Ketamine (100 mg/kg) and Xylazine (10 mg/ kg; CDMV) and then sacrificed. The number of nodules, as well as tumor weight and volume, were determined. In the second experiment, mice were injected with 5×10^6 SKOV3.ip1 control or mir-590 stable cells, and at 8, 16, and 23 days after cell inoculation, mice were anaesthetized and injected intraperitoneally with D-luciferin (150 mg/kg, Thermo Fisher Scientific), and bioluminescence signals were detected using an animal imager (ART Optix MX3).

Generation of *FOXA2* knockout cells

To knockout *FOXA2*, two single guide (sg)RNAs targeting human *FOXA2* (Supplementary Table S2), designed by the Zhang laboratory (28) and cloned into pLentiCRISPR v2, were purchased from GenScript. Lentiviral packaging plasmids (pMDLg/pRRE and pRSV-Rev) and the envelope plasmid (pMD2.G) was obtained from Addgene. To produce virus, 293T cells, seeded at a density of 2.5×10^6 cells/10-cm plate, were infected with 20 μg of each of the pLentiCRISPR v2 with or without FOXA2 sgRNA, 10 μg of pMDLg/pRRE, 5 μg of pRSV-Rev, and 6 μg of pMD2.G. Supernatants were collected and used to infect ES-2 and SKOV3.ip1 cells to generate the control with EV as well as the two *FOXA2* knockout lines: FOXAΔ1 and FOXAΔ2. After infection, cells were cultured with puromycin at a concentration of 1 μg/mL to select infected cells.

Published OnlineFirst May 10, 2018; DOI: 10.1158/0008-5472.CAN-17-3014

TCGA data analysis and bioinformatics

To investigate the correlation of FOXA2 and VCAN expression with multiple clinical attributes, portions of the TCGA Provisional dataset published on June 31, 2016, for ovarian serous cystadenocarcinoma (https://cancergenome.nih.gov) were downloaded from cBioPortal.org (29). This dataset contains 603 samples with associated clinical characteristics and 307 of those samples have undergone RNA-seq and Illumina HM27 methylation analysis, which were used in this study. Investigation of the preceding 2011 dataset was limited as it contained fewer samples, no RNA-seq/DNA methylation data, and far fewer clinical attributes. For these reasons, we report bioinformatical findings from the more comprehensive provisional dataset only. Sample data were aggregated from multiple files into a single comma delimited file using a custom C++ program (available from http://peng.lab.yorku.ca/bioinformatics-tools) compiled using Microsoft Visual Studio 2015 and analyzed in Microsoft Excel 2016. The analysis was independently completed at least twice to ensure a high degree of fidelity.

To determine the association between FOXA2 or VCAN and the clinical outcomes, samples were grouped into FOXA2 or VCAN "low" and "high" expression groups based on whether the expression levels were below or above, respectively, the mean value. These groups were then divided into subgroups based on the sample SDs from the mean (SD 1.0, SD 1.25, SD 1.5) where SD 0.0 represents all samples in the low or high group. In this way, subgroups represent increasing extremes of mRNA expression values. The following criteria were used to define the groups (Eq. A):

$$\begin{aligned} &If \quad x_i < \bar{x} - (s * m) \rightarrow \text{Low group} \\ &If \quad x_i > \bar{x} + (s * m) \rightarrow \text{High group} \end{aligned} \tag{A}$$

Where x_i represents each sample's FOXA2 or VCAN mRNA expression value, $\bar{x}$ the mean, s the sample standard deviation, and m the number of SDs from the mean; SD 1.0 is represented by $m = 1.0$. FOXA2 or VCAN mRNA expression groups and subgroups were calculated independently from each other.

To examine the effects of anticorrelated FOXA2 and VCAN mRNA expression samples, they were first assigned a Δ coefficient to represent the relative difference between FOXA2 and VCAN mRNA expression. mRNA expression values were converted to SDs from the mean (SDM) and then VCAN SDM was subtracted from FOXA2 SDM for each sample to calculate Δ (Eq. B):

$$\begin{aligned} &\Delta = \frac{x_i^{FOXA2} - \bar{x}^{FOXA2}}{s^{FOXA2}} - \frac{x_i^{VCAN} - \bar{x}^{VCAN}}{s^{VCAN}} \\ &\Delta < 0 \Rightarrow \downarrow FOXA2, \ \uparrow VCAN \\ &\Delta > 0 \Rightarrow \uparrow FOXA2, \ \downarrow VCAN \end{aligned} \tag{B}$$

The definition of variables is the same as those described for Eq. A.

Samples were shown or hidden based on the criteria above using conditional "IF" statements in Excel. This allowed manipulation of groups and subgroups by changing m (Eq. A) or ranges of Δ. Data retrieval was then based on samples passing the desired criteria and containing queried data (e.g., methylation) and then formatted to be copied to GraphPad. Binary data such as "Recurred/Progressed" and "Disease-free" were converted to 1 and 0, respectively. Likewise, clinical attributes for survival and invasion indicators were also converted to binary; "DECEASED" and "Yes" = 1, "LIVING" and "NO" = 0, respectively.

Statistical analysis

All *in vitro* experiments were done at least three times with at least triplicates in each group. The results are expressed as mean ± SEM in bar graphs and line graphs. Statistical analyses were performed using SigmaStat and GraphPad prism 6. Multiple groups were analyzed by one-way or two-way ANOVA, followed by Tukey *post hoc* test. Student *t* test was used for comparison between two groups. Clinical samples were presented as box–whisker plots and analyzed by Kruskal–Wallis test, followed by Wilcoxon rank test for multiple group comparison or Wilcoxon rank test when only two groups were compared. For TCGA clinical samples, binary data were analyzed using one-tailed Student *t* test. Kaplan–Meier survival and disease-free graphs were analyzed using the Mantel–Cox test; $P < 0.05$ was considered statistically significant.

Results

miR-590-3p is upregulated in ovarian cancer and promotes cell growth, migration, and invasion

Using EOC tissue samples collected at Mansoura Oncology Center (Supplementary Table S1A) and Ottawa Ovarian Cancer Tissue Bank (Supplementary Table S1B), we found that miR-590-3p levels in grade 2/3 ovarian tumors were significantly higher than in grade 1 tumors or normal ovarian tissues (Fig. 1A). Similarly, miR-590-3p levels were also upregulated in high-grade serous tumors when compared with tumors of low malignancy potential (Fig. 1B). In another histologic subtype of EOC, endometrioid ovarian cancer, high-grade tumors also had higher miR-590-3p levels than the low-grade ones (Supplementary Fig. S1A). Circulating miR-590-3p levels were also significantly higher in patients with EOC than in subjects with benign gynecologic disorders (Fig. 1C). To determine the effect of miR-590-3p on cell proliferation, migration, and invasion, EOC cell lines ES-2, SKOV3.ip1, and OVCAR3 were transiently transfected with miR-590-3p mimic, anti–miR-590-3p, or NCs. miR-590-3p significantly increased cell numbers (Fig. 1D; Supplementary Fig. S1B), migration, and invasion (Fig. 1E; Supplementary Fig. S1C–S1E). On the other hand, inhibition of miR-590-3p by anti–miR-590-3p resulted in a significant decrease in cell proliferation (Fig. 1D) and migration (Supplementary Fig. S1D).

Stable overexpression of mir-590 enhances tumor development and metastasis

To further investigate the function of miR-590-3p in EOC development, SKOV3.ip1 cells expressing luciferase, ES-2, and HEY cells stably transfected with mir-590 or its corresponding EV were generated (Supplementary Fig. S2A). Real-time PCR revealed that both miR-590-3p and miR-590-5p were significantly higher in cells transfected with mir-590, when compared with the EV (Supplementary Fig. S2B). Overexpression of mir-590 significantly enhanced cell proliferation (Fig. 1F), invasion (Fig. 1G), and colony formation (Fig. 1H; Supplementary Fig. S2C). To confirm that the observed effects of mir-590 were due to miR-590-3p and/or miR-590-5p overexpression, we transfected EV and mir-590 cells with anti–miR-590-3p,

Published OnlineFirst May 10, 2018; DOI: 10.1158/0008-5472.CAN-17-3014

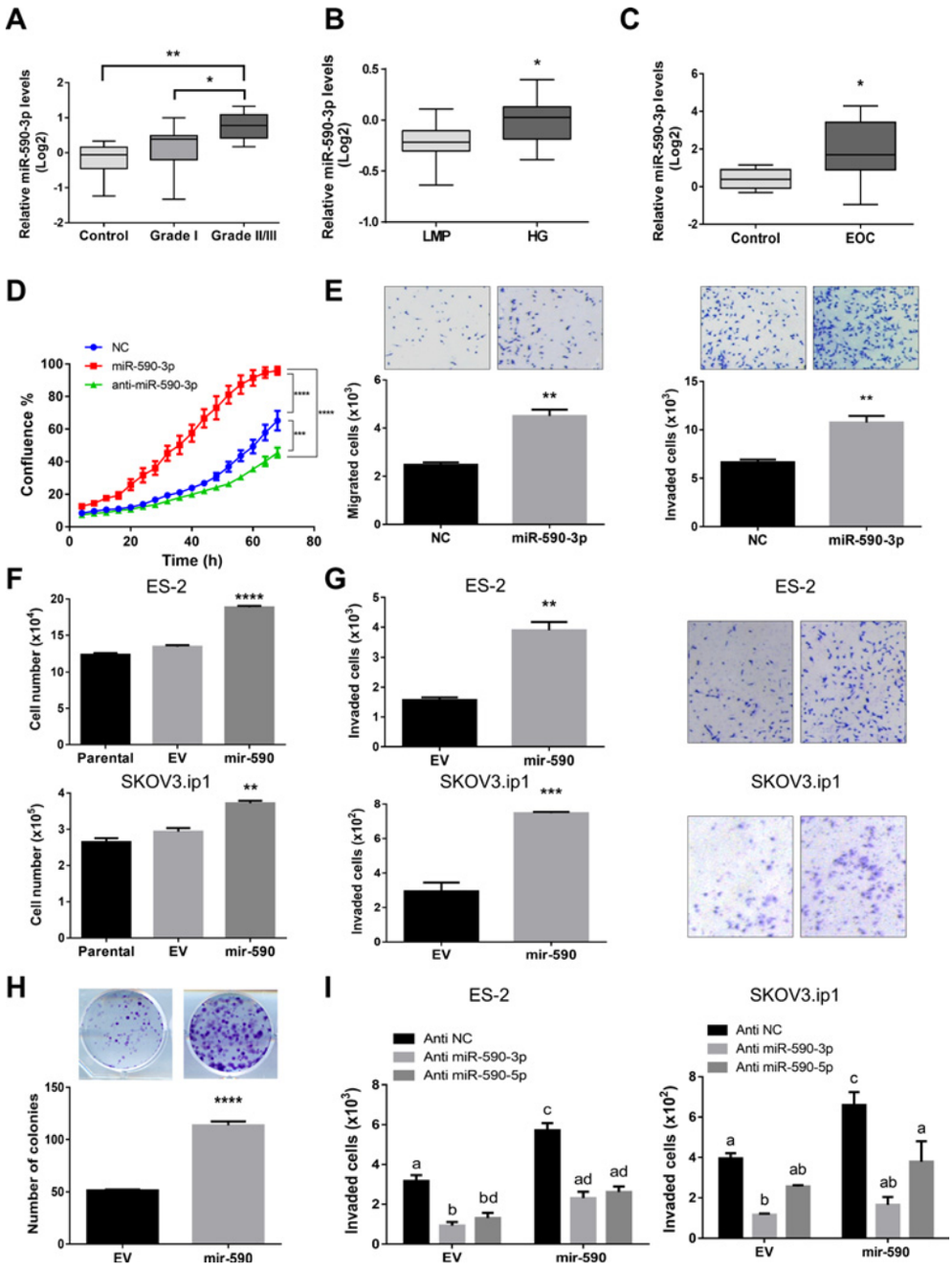

Figure 1.

miR-590-3p is upregulated in EOC and exerts tumor-promoting effects *in vitro*. **A,** miR-590-3p levels were elevated in higher grade EOC tumors compared with normal ovarian tissue or low-grade tumors. RNA was extracted from normal ovary ($n = 6$), grade 1 ($n = 11$), or grade 2/3 EOC samples ($n = 9$), and miR-590-3p level was determined by real-time PCR. **B,** miR-590-3p levels were higher in high-grade serous ovarian tumors (HG; $n = 14$) than in tumors with low malignancy potential (LMP; $n = 16$). **C,** Plasma miR-590-3p levels were significantly higher in patients with EOC ($n = 13$) than in subjects with benign gynecologic disorders ($n = 6$). Data in **A–C** are converted to $\log_2$ and plotted in box–whisker plots. **D,** miR-590-3p enhanced cell proliferation. SKOV3.ip1 cells were transiently transfected with NCs, miR-590-3p mimic, or anti–miR-590-3p. Cell confluency was monitored by IncuCyte for 68 hours ($n = 7$). **E,** miR-590-3p enhanced cell migration and invasion. ES-2 cells were transiently transfected with miR-590-3p or its NC, and transwell migration and invasion were determined at 24 hours after transfection ($n = 3$). **F,** Stable overexpression of mir-590 increased cell proliferation in both ES-2 and SKOV3.ip1 cells when compared with parental or control cells transfected with EV ($n = 3$). **G,** Cells overexpressing mir-590 invaded faster than cells expressing the EV ($n = 3$). **H,** In a clonogenic assay, cells overexpressing mir-590 formed more and larger colonies than the ones expressing the EV ($n = 3$). **I,** Effects of anti–miR-590-3p and anti–miR-590-5p on mir-590–induced cell invasion. ES-2 and SKOV3.ip1 cells stably transfected with EV or mir-590 were transiently transfected with anti–miR590-3p, anti–miR-590-5p, or their negative control (anti-NC). Transwell assays were performed ($n = 3$). Data represent median flanked by 25th and 75th percentiles (**A–C**) and mean ± SEM (**D–I**). *, $P < 0.05$; **, $P < 0.01$; ***, $P < 0.001$; ****, $P < 0.0001$. Different letters above bars denote statistical significance.

Published OnlineFirst May 10, 2018; DOI: 10.1158/0008-5472.CAN-17-3014

anti–mir-590-5p, or their nontargeting control. Both anti–miR-590-3p and anti–miR-590-5p reduced invasion in EV and mir-590 cells in ES2 cells. However, in SKOV3.ip1 cells, only anti–miR-590-3p had a significant effect of cell invasion in the EV control group (Fig. 1I).

To determine whether mir-590 affects tumor formation *in vivo*, ES-2 cells stably overexpressing mir-590 or its control vector were injected subcutaneously into female CD-1 nude mice and tumor size was measured over 21 days. The mir-590 cells formed significantly larger tumors at multiple time points measured (Fig. 2A). To examine the effect of mir-590 on metastasis, control and mir-590–expressing SKOV3.ip1 cells were injected intraperitoneally into the nude mice. It was observed that mice injected with mir-590 cells had a higher number of nodules throughout the peritoneal cavity (Fig. 2B) and formed larger tumors when compared with the control (Fig. 2C). Live animal imaging revealed that mice inoculated with mir-590 cells had stronger bioluminescent signals than mice injected with control cells (Fig. 2D).

miR-590-3p regulates FOXA2 and VCAN

To determine the molecular mechanisms by which mir-590 exerts tumor-promoting effects on EOC, cDNA microarray was performed. Genes that were either up- or downregulated by mir-590 by 2-fold or more were organized into a heatmap (Fig. 3A). Genes that were downregulated were analyzed for miR-590-3p/5p–binding sites using tools at microRNA.org. It was found that most of these genes have predicted miR-590-3p–binding sites and a few have predicted miR-590-5p sites (Supplementary Table S3A). Interrogation of the TCGA dataset revealed that most of the top mir-590–downregulated genes were underexpressed in ovarian cancer samples when compared with normal ovary (Supplementary Table S3A). Among them, FOXA2 is the most strongly downregulated gene that has a miR-590-3p–binding site and is also downregulated in the TCGA dataset (Supplementary Table S3A). On the other hand, among all upregulated genes by mir-590, VCAN is the most strongly upregulated in the TCGA database (Supplementary Table S3B) and known to play a role in EOC development (29). Therefore, we further investigated the expression, regulation, and function of FOXA2 and VCAN. Using the tumor samples collected from the Ovarian Cancer Tissue Bank at Ottawa Research Institute, we found that FOXA2 mRNA levels were significantly lower, whereas VCAN mRNA levels showed the opposite trend, in the high-grade tumors than in tumors of low malignancy potential (Fig. 3B). Real-time PCR and Western blotting confirmed that FOXA2 was downregulated in ES-2 and SKOV3.ip1 cells overexpressing mir-590 (Fig. 3C). FOXA2 mRNA levels were also significantly downregulated in HEY mir-590 stable cells (Supplementary Fig. S3A). In tumors collected from mice grafted with ES-2 cells, FOXA2 mRNA and protein levels were also downregulated (Supplementary Fig. S3B). Conversely, VCAN protein and mRNA levels were higher in mir-590 cells than in the vector controls (Fig. 3D).

miR-590-3p targets FOXA2

To confirm that miR-590-3p directly targets FOXA2, luciferase reporter assays were performed. Transient transfection of miR-590-3p mimic or stable transfection of mir-590 significantly reduced the luciferase activity (Fig. 3E). Transient transfection of miR-590-3p also reduced FOXA2 mRNA and protein levels, whereas anti–miR-590-3p enhanced FOXA2 protein levels in ES-2 cells (Fig. 3F). Similarly, transfection of the miR-590-3p mimic in HEY, SKOV3.ip1, and OVCAR3 cells decreased FOXA2 protein levels (Supplementary Fig. S3C).

FOXA2 exerts antitumor effects

To determine the role of FOXA2 in EOC development, we validated two siRNAs that decreased FOXA2 mRNA and protein levels (Fig. 4A). Transfection of these FOXA2 siRNAs in EOC cells accelerated proliferation (Fig. 4B) and invasion (Fig. 4C). To further confirm the role of FOXA2 in EOC cells, we used CRISPR/Cas9 gene editing tools to knockout *FOXA2* in both ES-2 and SKOV3.ip1 cells. Two sgRNAs were used to generate two populations of heterogeneous *FOXA2* knockout cells, designated as FOXAΔ1 and FOXAΔ2, respectively. *FOXA2* knockout diminished the expression of FOXA2 (Fig. 4D) and resulted in increased cell proliferation (Fig. 4E), migration (Fig. 4F), and invasion (Fig. 4G). Conversely, transient transfection of FOXA2 into several cell lines resulted in an inhibition of cell invasion (Fig. 4H; Supplementary Fig. S3D).

FOXA2 inhibits VCAN expression

Examination of a FOXA2 ChIP-seq dataset produced from mice revealed that *VCAN* was one of the genes enriched in FOXA2 antibody precipitated samples (30). Analysis of the human *VCAN* gene identified multiple potential FOXA2-binding sites on the promoter and gene body; therefore, we tested the possibility that FOXA2 regulates VCAN expression. In cells transiently transfected with siRNAs targeting FOXA2, there was an increase in VCAN mRNA levels (Fig. 5A). In contrast, overexpression of FOXA2 reduced VCAN mRNA (Fig. 5B) and protein (Supplementary Fig. S3D) levels. Furthermore, VCAN protein levels were increased in *FOXA2* knockout cells and the reintroduction of FOXA2 strongly downregulated VCAN levels, as revealed by Western blotting (Fig. 5C). Finally, ChIP-qPCR assays were performed in ES-2 and SKOV3.ip1 cells using three sets of primers designed to target the *VCAN* promoter site, a potential regulatory site, and a distal negative control region with no predicted FOXA2 binding site (NC; Fig. 5D, top). In FOXA2 antibody precipitated samples, enrichment of VCAN DNA was observed in the regions where FOXA2-binding sites were predicted when compared with the IgG group, while there was no difference between the IgG and FOXA2 antibody groups in the region that had no FOXA2-binding sites (Fig. 5D, bottom).

FOXA2 and VCAN are dysregulated in EOC

To further investigate the relationship between FOXA2 and VCAN and their significance in EOC development, we interrogated an ovarian cancer TCGA database. Initial sample-paired analysis of FOXA2 and VCAN mRNA levels displayed a slight negative correlation (Pearson: −0.1789, Spearman: −0.2249; Fig. 6A, left). To more closely evaluate the correlation between FOXA2 and VCAN mRNA levels and their possible effects on various clinical attributes, samples were divided into groups based on the deviation of their mRNA levels from the mean (Supplementary Fig. S4A and S4B). Groups were initially created in increments of 0.25 SDs. Because of the small sample sizes for groups with greater than 1.5 SD from the mean, they were excluded from the analysis. FOXA2 and VCAN mRNA levels were negatively correlated in most groups

Published OnlineFirst May 10, 2018; DOI: 10.1158/0008-5472.CAN-17-3014

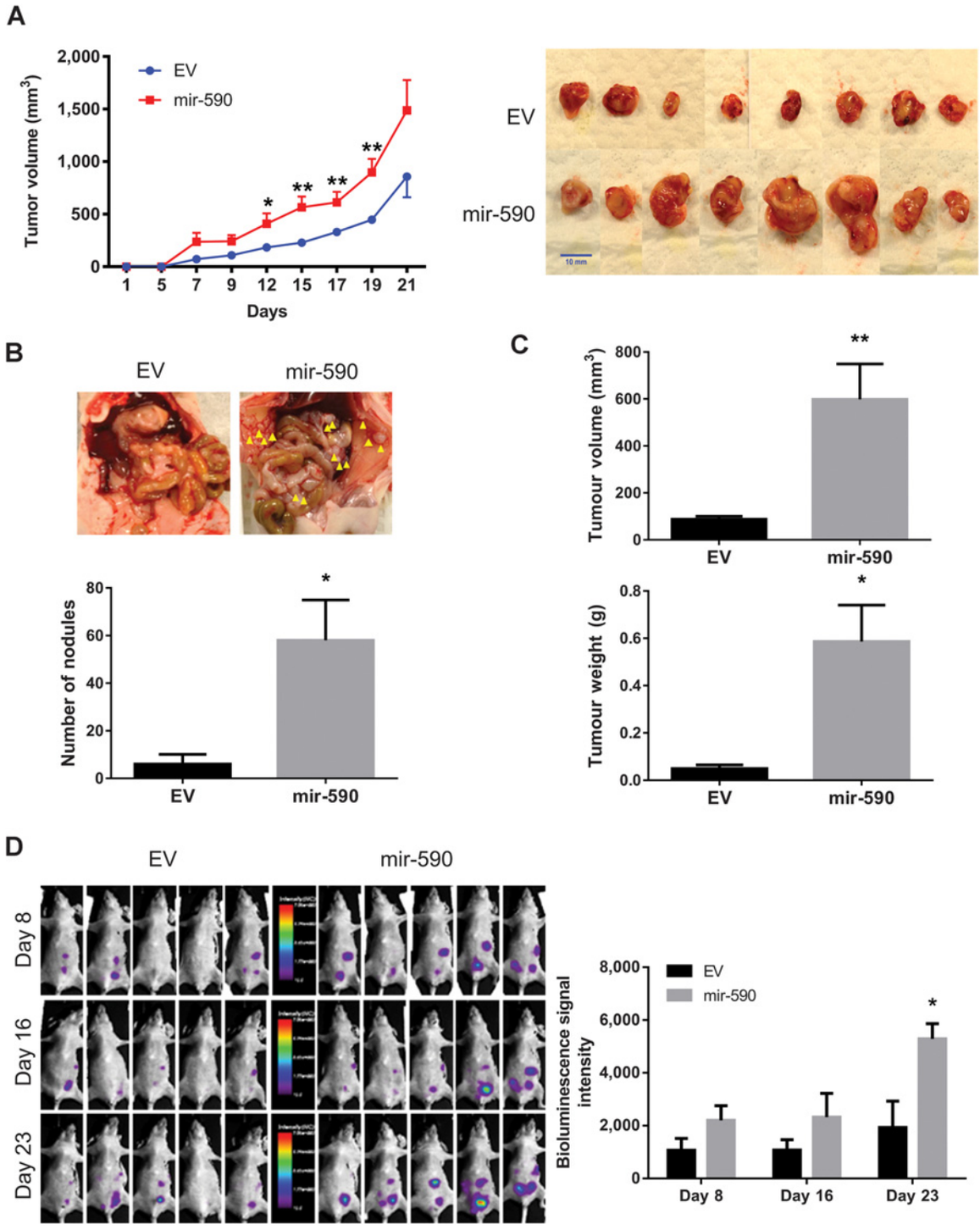

Figure 2.

mir-590 promotes tumor formation and metastasis *in vivo*. **A,** mir-590 accelerates tumor growth. ES-2 cells stably transfected with EV or mir-590 were injected subcutaneously into female CD-1 nude mice, and tumor volumes were measured ($n = 8$). **B** and **C,** mir-590 promotes tumor metastasis. SKOV3.ip1 cells stably transfected with luciferase and EV or miR-590 were injected intraperitoneally into CD-1 nude mice and the mice were examined at 70 days after tumor cell inoculation. The number of nodules (**B**) and total tumor volumes and weight (**C**) were significantly higher in mice injected with mir-590 cells when compared with the control. **D,** Bioluminescent imaging of mice inoculated with control or mir-590 cells. Mice were injected intraperitoneally with SKOV3.ip1 cells expressing the vector or mir-590 ($n = 5$). Bioluminescence images were taken at day 8 to day 23 after injection. Data, mean ± SEM. *, $P < 0.05$; **, $P < 0.01$.

Published OnlineFirst May 10, 2018; DOI: 10.1158/0008-5472.CAN-17-3014

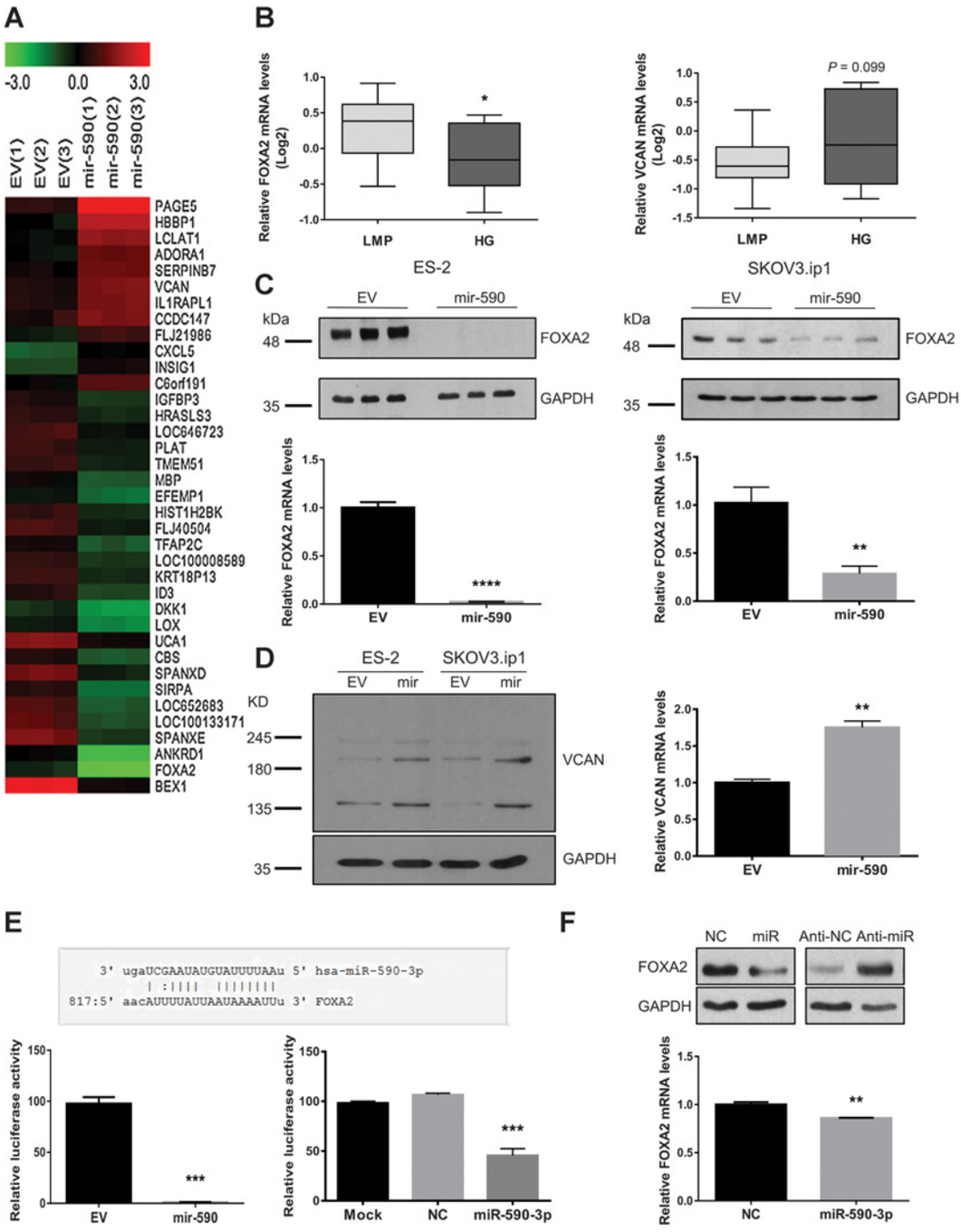

Figure 3.

Regulation of FOXA2 and VCAN by mir-590. **A,** Heatmap of genes regulated by mir-590 revealed by cDNA microarray. Total RNA extracted from ES-2 cells stably transfected with mir-590 or EV control were subjected to a cDNA microarray analysis. Genes that were ≥2-fold down- or upregulated by mir-590 were included in the heatmap. **B,** FOXA2 mRNA levels (left) were significantly lower, whereas VCAN mRNA levels (right) showed an opposite trend in high-grade serous ovarian tumors (HG; $n = 13$) than in tumors with low malignancy potential (LMP; $n = 15$). **C,** Confirmation of FOXA2 downregulation by mir-590 using real-time PCR and Western blotting in both ES-2 and SKOV3.ip1 stable cells. **D,** Upregulation of VCAN by mir-590. Overexpression of mir-590 resulted in an increase in VCAN protein levels in both ES-2 and SKOV3.ip1 cells (left). Real-time PCR (right) revealed higher VCAN mRNA levels in mir-590–expressing in ES-2 cells ($n = 3$). **E,** FOXA2 is a target of miR-590-3p. A predicted miR-590-3p–binding site was found on FOXA2 3′ UTR. A luciferase reporter construct containing FOXA2 3′ UTR was generated. In ES-2 cells stably transfected with mir-590 (left), or transiently transfected with miR-590-3p (right), the luciferase activity was significantly decreased ($n = 3$). **F,** Transient transfection of miR-590-3p decreased FOXA2 mRNA levels ($n = 3$) and the protein levels, whereas transfection of anti–miR-590-3p increased FOXA2 protein levels. Statistical analyses were performed using Wilcoxon rank test (**B**), ANOVA/Tukey test (**E**, right), or t test (all others). *, $P < 0.05$; **, $P < 0.01$; ***, $P < 0.001$; ****, $P < 0.0001$ versus their respective controls.

Published OnlineFirst May 10, 2018; DOI: 10.1158/0008-5472.CAN-17-3014

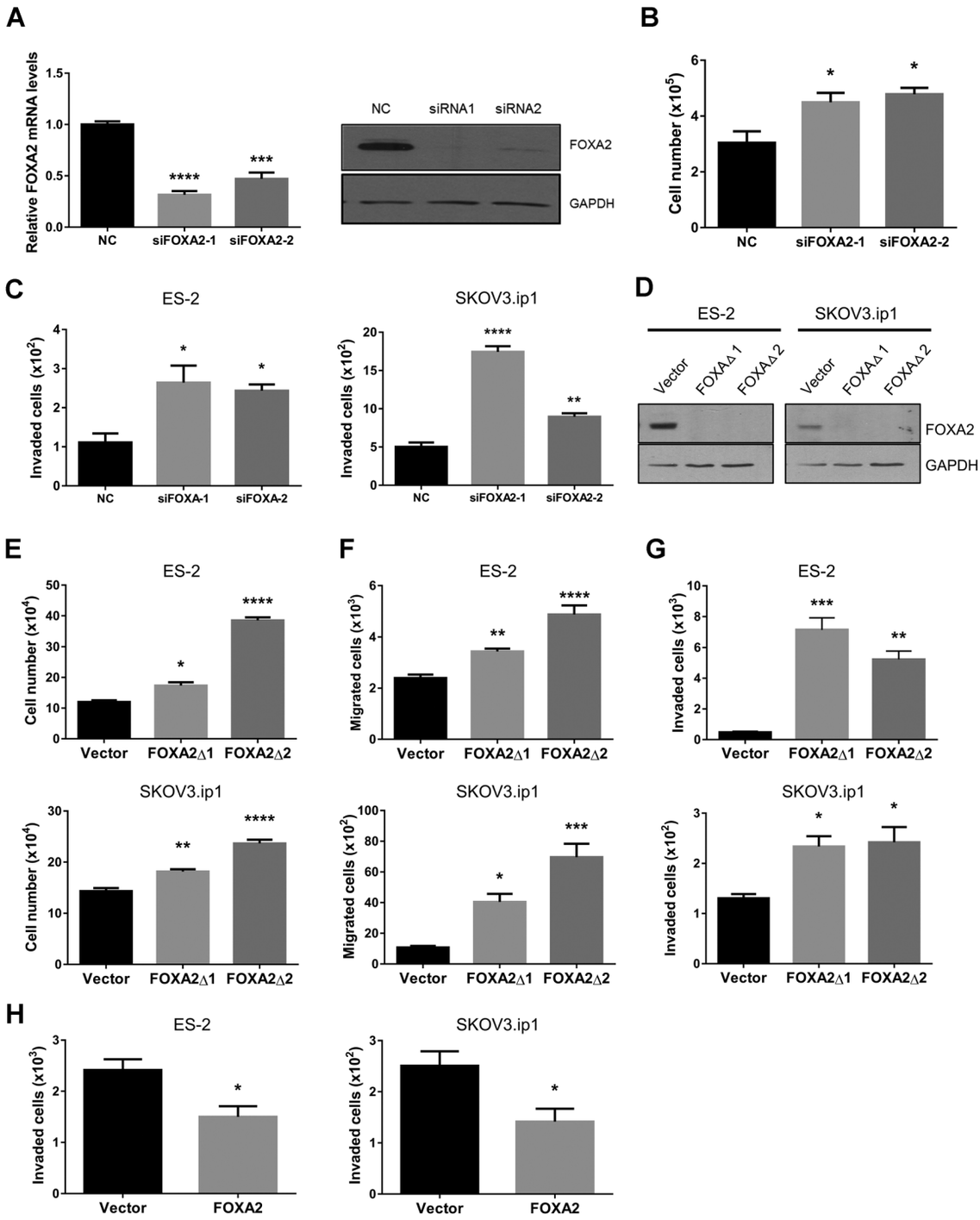

Figure 4.

FOXA2 exerts antitumor effects in EOC cells. **A,** Validation of two different siRNAs targeting FOXA2. In ES-2 cells transfected with FOXA2 siRNAs, FOXA2 mRNA and protein levels were reduced, when compared with cells transfected with a nontargeting siRNA (NC). Total RNA and proteins were extracted at 48 hours after transfection. **B,** Knockdown of FOXA2 increased ES-2 cell proliferation. Cell numbers were measured 48 hours posttransfection. **C,** Knockdown of FOXA2 increased cell invasion in ES-2 and SKOV3.ip1 cells. Cells were transfected with NC or one of the FOXA2 siRNAs, and 24 hours posttransfection, cells were resuspended and an equal number of cells were then placed on the top chamber of the transwell inserts. Invaded cells were counted at 18 hours after plating. **D,** Generation of *FOXA2* knockout cells using CRISPR/Cas9. Two gRNAs were used and both eliminated FOXA2 protein in ES-2 and SKOV3.ip1 cells, as confirmed by Western blotting. **E–G,** Knockout of *FOXA2* increased cell proliferation (**E**), migration (**F**), and invasion (**G**). **H,** Transient transfection of FOXA2 plasmid into ES-2 and SKOV3.ip1 cells resulted in a decrease in cell invasion. Data, mean ± SEM ($n = 3$). *, $P < 0.05$; **, $P < 0.01$; ***, $P < 0.001$; ****, $P < 0.0001$ versus controls.

Published OnlineFirst May 10, 2018; DOI: 10.1158/0008-5472.CAN-17-3014

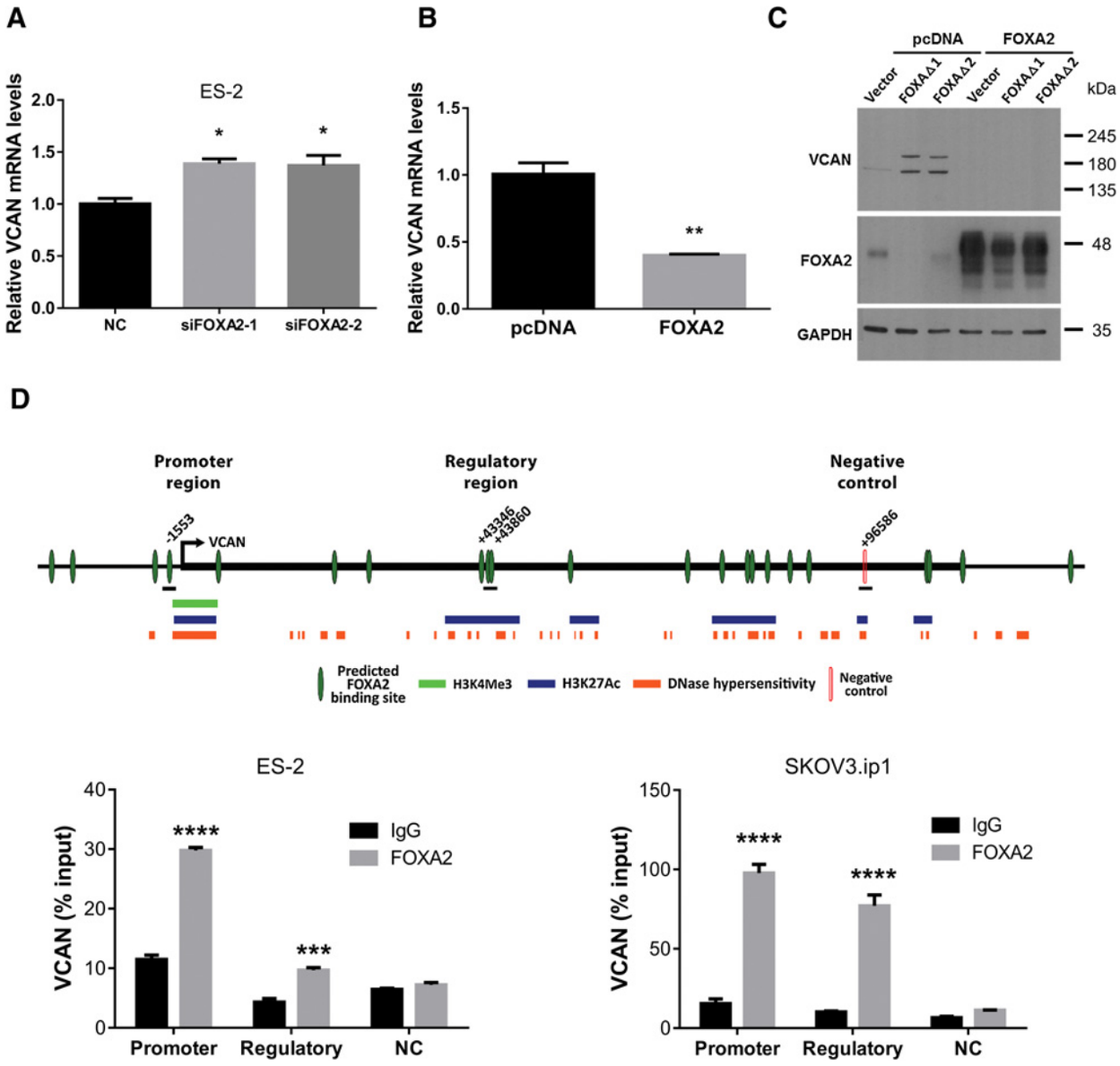

Figure 5.

FOXA2 regulates VCAN expression. **A,** ES-2 cells transfected with FOXA2 siRNAs increased the mRNA level of VCAN. **B,** In SKOV3.ip1 cells, transient transfection of FOXA2 decreased the mRNA level of VCAN. **C,** Knockout of *FOXA2* in ES-2 cells increased VCAN protein levels, but this effect was reversed by overexpression of FOXA2. **D,** FOXA2 binds to *VCAN* gene. Top, consensus FOXA2-binding sites were predicted in the *VCAN* promoter and within the gene body. Most of these predicted sites overlap DNA regions with histone modifications associated with regulatory potential and DNase hypersensitivity regions. Three pairs of primers were designed. The first pair targets the FOXA2-binding site in the promoter region (promoter; −1553 bp), the second pair spans two intragenic binding sites in a region with regulatory features (regulatory; +43346, +43860), and a distal region with no predicted FOXA2-binding site, which serves as a negative control (NC; +96586). Bottom, ChIP-qPCR was performed using FOXA2 antibody or IgG in both ES-2 and SKOV3.1p1 cells. VCAN DNA was enriched in the promoter, and to a lesser extent, the regulatory region (in ES-2), but not in the negative control. Data, mean ± SEM (**A**, **B**, and **D**; $n = 3$). *, $P < 0.05$; **, $P < 0.01$; ***, $P < 0.001$; ****, $P < 0.0001$ versus controls as analyzed by ANOVA/Tukey test (**A**) or *t* test (**B** and **D**).

(Supplementary Fig. S4C). We adapted the minimal signal method from Adorno and colleagues (31) to produce a delta (Δ) coefficient for each sample such that a $\Delta < 0$ represents samples with relatively low FOXA2 and high VCAN mRNA levels and oppositely for $\Delta > 0$ (Fig. 6A, right; Supplementary Fig. S4D). Methylation of both FOXA2 and VCAN promoters was also examined. FOXA2 mRNA levels were negatively correlated with promoter methylation levels (Pearson: −0.3672, Spearman: −0.4232, $P < 0.0001$). Importantly, FOXA2 promoter methylation was positively correlated with VCAN mRNA levels (Pearson: 0.1750, Spearman: 0.3934, $P < 0.0001$; Fig. 6B). These samples were then divided into low or high

Published OnlineFirst May 10, 2018; DOI: 10.1158/0008-5472.CAN-17-3014

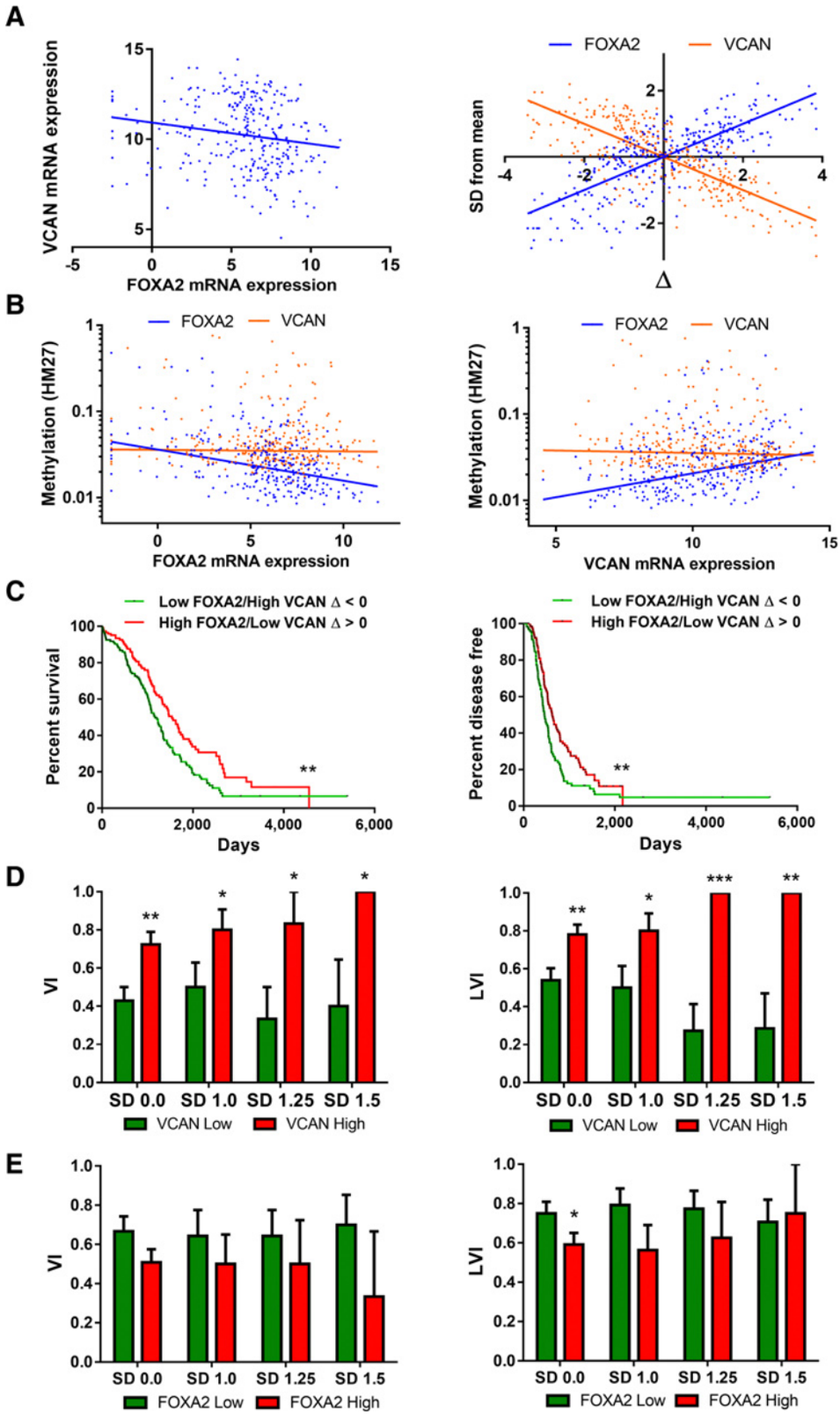

Figure 6.
Analysis of FOXA2 and VCAN expression patterns in EOC tumors. **A,** FOXA2 and VCAN mRNA levels are negatively correlated in ovarian cancer samples. Left, sample-paired FOXA2 and VCAN mRNA levels ($\log_2$; RNA-Seq V2 RSEM) in TCGA ovarian serous cystadenocarcinoma dataset were negatively correlated ($n = 307$). Pearson, -0.1789; $P = 0.017$. Spearman, -0.2249; $P < 0.0001$. Right, FOXA2 and VCAN mRNA levels were converted to their distance from the mean in SDs (*Z*-score). Delta (Δ) values were calculated for each tumor sample using SD from the mean of FOXA2 and VCAN mRNA expressions to group each sample based on the degree of relative anticorrelation in their expression. Delta values less than zero correlate with relatively low FOXA2 and high VCAN mRNA expression, whereas values greater than zero correlate with relatively high FOXA2 and low VCAN mRNA expression. **B,** Left, FOXA2 mRNA expression was negatively correlated with *FOXA2* promoter methylation (Pearson, -0.3672; $P < 0.0001$; Spearman, -0.4232; $P < 0.0001$). Right, VCAN mRNA expression was positively correlated with *FOXA2* promoter methylation (Pearson, 0.1750; $P = 0.0024$; Spearman, 0.3934; $P < 0.0001$). **C,** Kaplan–Meier graphs of either percent survival (left) or percent disease-free (right) were plotted using delta groups less than or greater than zero. Delta values less than zero correlate with relatively low FOXA2 and high VCAN mRNA expression, whereas values greater than zero correlate with relatively high FOXA2 and low VCAN mRNA expression. Median survival was significantly greater in the $\Delta > 0$ group based on the log-rank (Mantel–Cox) test; $P = 0.0036$. $\Delta < 0$: 1,169.7 d ($n = 159$); $\Delta > 0$: 1,539.3 d ($n = 147$). The median time of disease-free status was significantly longer in the $\Delta > 0$ group based on the log-rank (Mantel–Cox) test; $P = 0.0029$. $\Delta < 0$: 455.4 d ($n = 159$); $\Delta > 0$: 624.9 d ($n = 147$). **D** and **E,** Association between the proportion of subjects that were positive for vascular (VI; left) and lymphovascular (LVI; right) invasion indicators and VCAN or FOXA2 mRNA levels. Data, mean ± SEM. *, $P < 0.05$; **, $P < 0.01$; ***, $P < 0.001$.

Published OnlineFirst May 10, 2018; DOI: 10.1158/0008-5472.CAN-17-3014

groups based on their SD from their mean values (Supplementary Fig. S5A and S5B), and using delta groups with combined FOXA2 and VCAN expression profiles (Supplementary Fig. S5C). *FOXA2* promoter methylation was found to be increasingly polarized as both FOXA2 and VCAN mRNA levels moved further from the mean (Supplementary Fig. S5A and S5C, left). In contrast, VCAN promoter methylation was not correlated with either FOXA2 or VCAN mRNA levels (Supplementary Fig. S5B and S5C), except for the SD 1.5 high FOXA2 group (Supplementary Fig. S5B).

Next, we investigated the survival rates and disease-free statuses using the SD groups. We observed a trend that high FOXA2 (Supplementary Fig. S6A) or low VCAN (Supplementary Fig. S6B) is associated with longer survival. To determine whether the degree of negative correlation between FOXA2 and VCAN is associated with patient survival, we examined the delta coefficient groups. In the $\Delta > 0$ group that has high FOXA2 and low VCAN mRNA levels, both survival rates and disease-free statuses were increased with a median survival increase from 1,170 to 1,539 days ($P = 0.0036$) and disease-free period from 455 to 624 days ($P = 0.0029$; Fig. 6C). Interestingly, when examining the degree of vascular (VI) and lymphovascular (LVI) invasion, there was a significant positive correlation with VCAN and a trend of negative correlation with FOXA2 mRNA levels (Fig. 6D).

The FOXA2–VCAN pathway mediates mir-590 effect

To confirm that the downregulation of FOXA2 and upregulation of VCAN contribute to the tumor-promoting effects of mir-590, rescue experiments were performed. We observed that overexpression of FOXA2 significantly reduced the ability of mir-590 to enhance cell migration and invasion (Fig. 7A). In addition, we determined whether silencing of VCAN would abolish the tumor-promoting effects of *FOXA2* knockout. *FOXA2* knockout cells expressed higher VCAN levels and significantly increased cell migration and invasion. However, these effects were significantly reduced when VCAN was knocked down in SKOV3.ip1 (Fig. 7B) and ES-2 (Fig. 7C) cells. Knockdown of VCAN also reduced the stimulatory effects of mir-590 on cell proliferation and invasion (Fig. 7D).

Discussion

In this study, we provided strong evidence to support a tumor-promoting role of miR-590-3p in ovarian cancer cells. We demonstrated that overexpression of miR-590-3p or its precursor, mir-590, significantly increased cell proliferation, migration, invasion, and colony formation *in vitro*. In addition, mir-590 promoted tumor growth and metastasis *in vivo*. Moreover, miR-590-3p levels were significantly elevated in high-grade EOC tumors when compared with normal ovaries or lower grade tumors. Finally, miR-590-3p plasma levels were higher in patients with EOC than in subjects with benign gynecologic disorders. These findings suggest that higher miR-590-3p is associated with a more aggressive disease.

Although the role of miR-590-3p in EOC has not previously been established, several studies have reported both tumor-promoting and tumor-suppressive effects of miR-590-3p in other types of cancer. For example, miR-590-3p promotes cell proliferation and invasion in T-cell acute lymphoblastic leukemia by inhibiting RB1 (6) and in colorectal cancer by targeting the Hippo pathway (7) and by promoting β-catenin signaling (32). Similarly, tumor-promoting effects of miR-590-3p were observed in glioblastoma (33). In contrast, miR-590-3p suppresses hepatocellular carcinoma growth (34) and inhibits proliferation and migration in bladder cancer cells (35). In this study, we demonstrated that miR-590-3p enhanced colony formation, cell proliferation, migration, and invasion *in vitro*, and stimulated tumor growth and metastasis *in vivo*. These findings strongly support a tumor-promoting role of miR-590-3p in EOC. The differential role of miR-590-3p reported in different types of cancer is likely due to the differential targeting of genes by miR-590-3p and/or differential effects of its target genes. Indeed, we examined several reported target genes responsible for the antitumor effects of miR-590-3p, such as ZEB1 and ZEB2, and did not observe an inhibition by miR-590-3p or mir-590 in EOC cells. On the other hand, we found that DKK1, which was reported to be targeted by miR-590-3p in colon cancer (32), was strongly downregulated in our mir-590 cells. In addition, the tumor-promoting effects of mir-590 observed in our study could also be attributed to miR-590-5p overexpression. We observed that both anti–miR-590-3p and anti–miR-590-5p attenuated the effect of mir-590, suggesting that miR-590-5p is also involved in EOC development.

In this study, we identified FOXA2 as a direct target of miR-590-3p and provided several lines of evidence to support a tumor-suppressive role of FOXA2 in EOC. First, FOXA2 mRNA levels were significantly downregulated in high-grade tumors when compared with tumors of low malignancy potential, suggesting that FOXA2 expression is associated with a less aggressive phenotype. Second, silencing of FOXA2 expression promoted cell proliferation, migration, and invasion, whereas overexpression of FOXA2 had the opposite effects. Finally, higher FOXA2 appeared to be associated with better patient survival. These findings are consistent with a previous study that identified FOXA2 as one of the 26 genes enriched in differentiated ovarian tumors with better prognosis (36). The results are also in agreement with studies in lung cancer, which demonstrate that FOXA2 is a strong inhibitor of metastasis with decreased expression levels during cancer progression (12, 13). Similarly, FOXA2 has been reported to suppress EMT and metastasis in breast cancer (15). However, FOXA2 expression in triple-negative/basal-like breast carcinoma is positively associated with relapse and promotes cancer development (16). Interestingly, in a mouse model of liver cancer, Foxa2 and Foxa1 suppress or promote liver cancer development, depending on whether they interact with estrogen receptor α (ERα) or androgen receptor, respectively (17). This study also revealed that SNPs at FOXA2-binding sites, which impair the binding of both FOXA2 and ERα to their targets, correlate with liver cancer development in women. Thus, it is possible that the dual function of FOXA2 in cancer development is dependent, at least in part, on its interacting partners. It remains to be determined which factor(s) FOXA2 interacts with to exert the tumor-suppressive effects in EOC.

Findings from the current study identified a novel relationship between FOXA2 and VCAN. We demonstrated that knockdown or knockout of *FOXA2* enhanced, whereas overexpression of FOXA2 reduced, VCAN expression. In addition, ChIP-qPCR results showed that FOXA2 bound to the *VCAN* gene. These findings strongly suggest that FOXA2 is a transcriptional repressor of VCAN. This notion is further supported by the expression patterns of FOXA2 and VCAN in EOC tumor

Published OnlineFirst May 10, 2018; DOI: 10.1158/0008-5472.CAN-17-3014

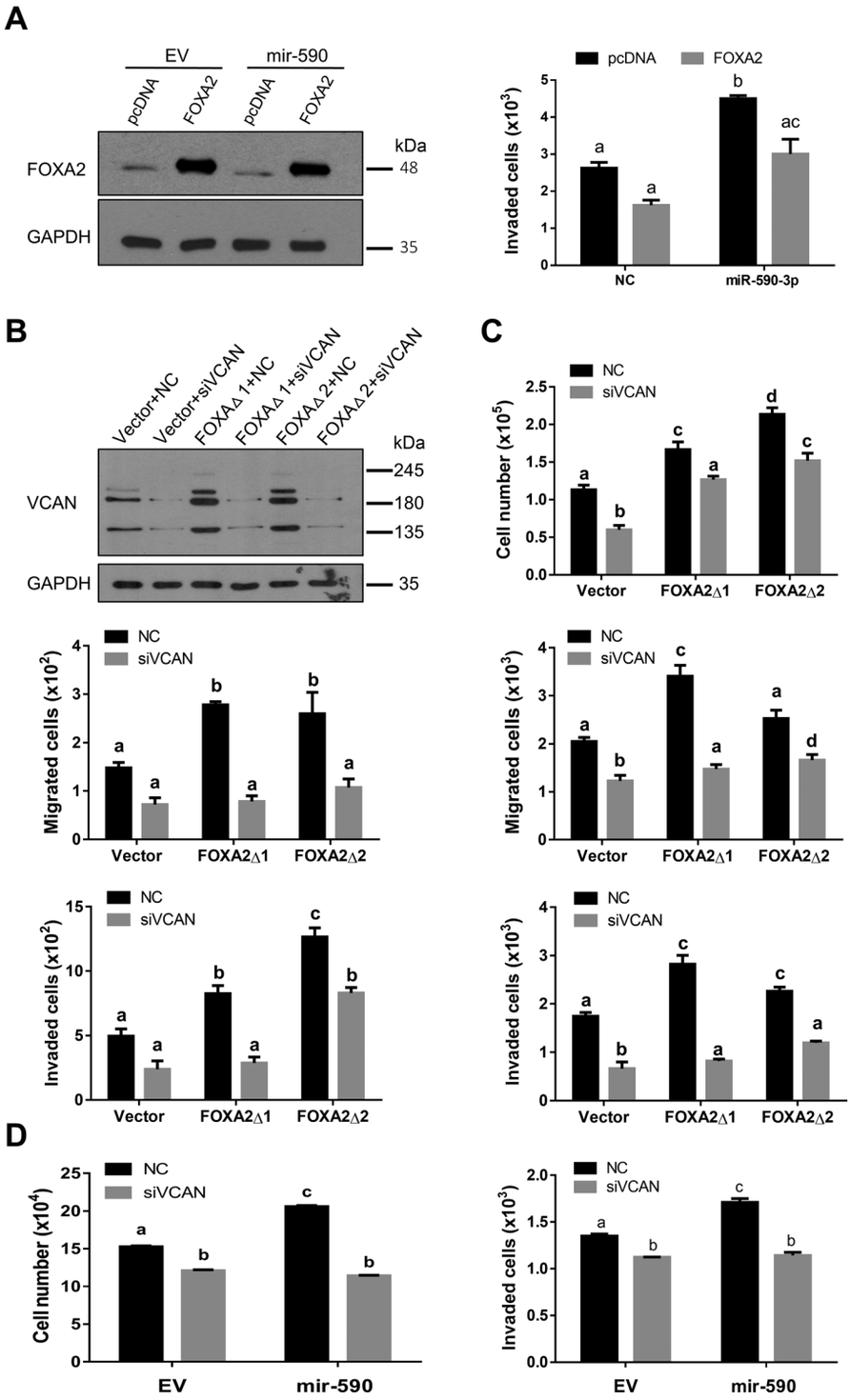

Figure 7.

FOXA2 and VCAN mediate the effects of mir-590 in EOC cells. **A,** Overexpression of FOXA2 in SKOV3.ip1 cells reversed the effect of mir-590. Control (EV) or mir-590 stable cells were transfected with either the control plasmid vector (pcDNA) or FOXA2-expressing plasmid. Overexpression of FOXA2 reduced the effects of mir-590 on invasion. **B,** Silencing of VCAN by siRNA reversed the effects of *FOXA2* knockout. Top, confirmation of VCAN knockdown by siRNA using Western blot analysis. Knockdown of VCAN significantly reduced cell migration (middle) and invasion (bottom) in *FOXA2* knockout SKOV3.ip1 cells. **C,** In ES-2 cells, knockdown of VCAN attenuated the effect of *FOXA2* knockout on cell proliferation (top), migration (middle), and invasion (bottom). **D,** Knockdown of VCAN reduced the effects of mir-590 on cell proliferation (left) and invasion (right). Statistical analyses were performed using ANOVA/Tukey test and groups significantly different from each other are denoted by a different letter.

Published OnlineFirst May 10, 2018; DOI: 10.1158/0008-5472.CAN-17-3014

samples, which reveal a negative correlation between FOXA2 and VCAN mRNA levels. Importantly, we found that high FOXA2 and low VCAN mRNA levels in the same tumor sample were significantly associated with longer patient survival. Knockdown of VCAN reduced cell proliferation, migration, and invasion, supporting a tumor-promoting role of VCAN. It has been reported that VCAN can be produced from both ovarian cancer cells (37) and cancer-associated fibroblasts (20). Because the tumor samples in the TCGA database most likely contain both cancer and fibroblastic stromal cells, it remains to be determined whether a negative relationship between FOXA2 and VCAN exists in both cancer and stromal cells.

Several isoforms of VCAN, namely V0, V1, V2, and V3, with molecular weights of approximately 370, 263, 180, and 74 kDa, respectively, are generated by alternative splicing (38). Although V0 and V1 isoforms promote cancer development in many types of cancers, V2 and V3 isoforms have been reported to have antitumor effects (39). Studies in EOC tumor samples revealed that V1 is the most abundant isoform (19). The VCAN antibody that we used in this study detected several bands with molecular weights between 245 and 135 kDa. The intensity of all bands was reduced by the VCAN siRNA, indicating that they are all related to VCAN. Based on the molecule weight, the V3 isoform is not detected in our Western blots. It has been reported that in several EOC cell lines, including SKOV3 and OVCAR3, V2 isoform is not expressed (37). In addition, V1 isoform can be processed into smaller fragments (40). Thus, it is possible that miR-590-3p and FOXA2 regulate the expression of V1, and possibly V0.

Although it is widely believed that EOC metastasis occurs mainly within the peritoneal cavity (2), recent studies suggest that ovarian cancer cells can also spread via hematogenous metastasis (3). In our analysis of VCAN levels in patients with ovarian cancer, we found that high VCAN levels were positively correlated with an increase in vascular and lymphovascular invasion indicator in the same samples. These observations, together with the finding that VCAN promotes invasion (20) and metastasis (37) in ovarian cancer, raise the interesting possibility that VCAN may play an important role in promoting hematogenous and lymphatic dissemination of EOC tumors.

One of the limitations of this study is the comparison of gene expression between tumor tissues and normal ovary or between tumors of different grades. EOC is a highly heterogeneous disease consisting of at least five histologic subtypes, high-grade serous carcinoma (HGSC), endometrioid carcinoma, clear cell carcinoma (CCC), low-grade serous carcinoma, and mucinous carcinoma, with HGSC accounting for 70% to 74% of EOC (41). The different subtypes of EOC have distinct molecular features and tissue origins. It is believed that most HGSC originate from the fallopian tube epithelium, but some HGSCs may still arise from the ovarian surface epithelium (41). The TCGA database contains data from ovarian serous cystadenocarcinoma and normal ovary, and therefore, we compared the expression of genes regulated by mir-590 between these two groups. This comparison is not ideal as most ovarian carcinomas originate outside the ovary. We therefore also compared miR-590-3p, FOXA2, and VCAN levels between the high-grade and low-grade tumors. However, such comparisons also have drawbacks because high- and low-grade tumors may have different tissue origins. Thus, we cannot exclude the possibility that the difference in gene expression patterns observed between carcinoma and normal ovary or between different grades of tumors may reflect the different tissue origins. Nevertheless, the higher level of miR-590-3p in the more aggressive higher grade tumors, together with the finding that miR-590-3p promotes EOC cell invasion *in vitro* and metastasis *in vivo*, strongly suggests that miR-590-3p expression is associated with a more aggressive behavior of EOC. Our finding that plasma miR-590-3p levels were higher in patients with ovarian cancer than in control subjects further supports the notion that miR-590-3p is dysregulated during ovarian cancer development. However, it is not clear which factor(s) triggers the dysregulation of miR-590-3p during EOC development. A recent study reported that hypoxia increased miR-590-5p expression to promote colon cancer metastasis (42). It remains to be investigated whether miR-590-3p is also induced by hypoxia.

ES-2 and SKOV3 cells are commonly used in ovarian cancer research. Most of the experiments in this study were conducted using ES-2 and SKOV3.ip1. SKOV3.ip1 was established from the ascites of a nude mouse injected intraperitoneally with SKOV3 cells (43) that is known to be a model for endometrioid carcinoma (41). ES-2 originated from a CCC (44); however, a recent study has placed ES-2 into the category of probably HGSC (45). ES-2 is now listed as a cell line with mixed feature (41). Because most of the samples used for bioinformatics analysis to determine the correlation between FOXA2/VCAN and patient survival were done using the TCGA dataset, which likely contains mostly HGSC tumors, we repeated some of the experiments in a HGSC cell line, OVCAR3 (41) and observed that, similar to ES-2 and SKOV3.ip1 cells, miR-590-3p enhanced cell invasion and decreased FOXA2 expression. On the other hand, FOXA2 suppressed cell invasion and inhibited VCAN expression. We have also obtained limited, but similar, results from the HEY cell line, which has also been used as a model for HGSC (46). Based on these findings, it is possible that the miR-590-3p–FOXA2–VCAN pathway is preserved in multiple subtypes of EOC.

In summary, our study characterizes a previously unreported role of miR-590-3p in promoting EOC development in part by targeting FOXA2. We also provide evidence to support a novel tumor-suppressive role of FOXA2 in EOC via inhibition of VCAN expression. Finally, our findings that low FOXA2/high VCAN mRNA levels in EOC tumors correlate with poor survival suggest that these genes may be prognostic markers for this deadly disease.

Disclosure of Potential Conflicts of Interest

No potential conflicts of interest were disclosed.

Authors' Contributions

Conception and design: M. Salem, J.A. O'Brien, S. Bernaudo, A. Amleh, C. Peng
Development of methodology: M. Salem, J.A. O'Brien, H. Shawer, G. Ye, A. Amleh, S.N. Krylov
Acquisition of data (provided animals, acquired and managed patients, provided facilities, etc.): S. Bernaudo, H. Shawer, G. Ye, A. Amleh, B.C. Vanderhyden, B. Refky
Analysis and interpretation of data (e.g., statistical analysis, biostatistics, computational analysis): M. Salem, J.A. O'Brien, H. Shawer, J. Brkić, A. Amleh, S.N. Krylov, C. Peng
Writing, review, and/or revision of the manuscript: M. Salem, J.A. O'Brien, S. Bernaudo, J. Brkić, B.C. Vanderhyden, B.B. Yang, S.N. Krylov, C. Peng
Administrative, technical, or material support (i.e., reporting or organizing data, constructing databases): M. Salem, G. Ye
Study supervision: G. Ye, A. Amleh, C. Peng

Acknowledgments

This study was supported by grants from Canadian Institutes of Health Research (MOP-89931 and PJT-153146) and Canada Foundation for Innovation/Ontario Research Fund (project #35611) to C. Peng. J.A. O'Brien was a recipient of graduate scholarships from Ontario Graduate Scholarship (OGS) and York University. S. Bernaudo was a recipient of graduate scholarships from NSERC, OGS, and York University. J. Brkić was a recipient of graduate scholarships from QEII-GSST, OGS, and York University. The research performed in Egypt was supported by the American University in Cairo Internal Faculty Research Grant to A. Amleh and Graduate Student Research Grant to H. Shawer. We thank Dr. J. Liu for her help in statistical analyses of the clinical data, Dr. M.C. Hung for SKOV3.ip1 cells, E. Macdonald and the tumour bank at Ottawa Hospital Research Institute for providing the ovarian cancer samples, and Dr. Z. Wu for critical comments. The Ottawa Ovarian Cancer Tissue Bank is supported in part by Ovarian Cancer Canada. We are grateful to all patients who donated the samples.

The costs of publication of this article were defrayed in part by the payment of page charges. This article must therefore be hereby marked *advertisement* in accordance with 18 U.S.C. Section 1734 solely to indicate this fact.

Received October 3, 2017; revised March 23, 2018; accepted May 3, 2018; published first May 10, 2018.

References

1. Coleman RL, Monk BJ, Sood AK, Herzog TJ. Latest research and treatment of advanced-stage epithelial ovarian cancer. Nat Rev Clin Oncol 2013; 10:211–24.
2. Lengyel E. Ovarian cancer development and metastasis. Am J Pathol 2010;177:1053–64.
3. Pradeep S, Kim SW, Wu SY, Nishimura M, Chaluvally-Raghavan P, Miyake T, et al. Hematogenous metastasis of ovarian cancer: rethinking mode of spread. Cancer Cell 2014;26:77–91.
4. Lin S, Gregory RI. MicroRNA biogenesis pathways in cancer. Nat Rev Cancer 2015;15:321–33.
5. Eulalio A, Mano M, Ferro MD, Zentilin L, Sinagra G, Zacchigna S, et al. Functional screening identifies miRNAs inducing cardiac regeneration. Nature 2012;492:376–81.
6. Miao M-h, Ji X-q, Zhang H, Xu J, Zhu H, Shao X-j. miR-590 promotes cell proliferation and invasion in T-cell acute lymphoblastic leukaemia by inhibiting RB1. Oncotarget 2016;7:39527–34.
7. Sun ZQ, Shi K, Zhou QB, Zeng XY, Liu J, Yang SX, et al. MiR-590-3p promotes proliferation and metastasis of colorectal cancer via Hippo pathway. Oncotarget 2017;8:58061–71.
8. Pang H, Zheng Y, Zhao Y, Xiu X, Wang J. miR-590-3p suppresses cancer cell migration, invasion and epithelial–mesenchymal transition in glioblastoma multiforme by targeting ZEB1 and ZEB2. Biochem Biophys Res Commun 2015;468:739–45.
9. Keller A, Backes C, Leidinger P, Kefer N, Boisguerin V, Barbacioru C, et al. Next-generation sequencing identifies novel microRNAs in peripheral blood of lung cancer patients. Mol Biosyst 2011;7:3187–99.
10. Friedman JR, Kaestner KH. The Foxa family of transcription factors in development and metabolism. Cell Mol Life Sci 2006;63:2317–28.
11. Vorvis C, Hatziapostolou M, Mahurkar-Joshi S, Koutsioumpa M, Williams J, Donahue TR, et al. Transcriptomic and CRISPR/Cas9 technologies reveal FOXA2 as a tumor suppressor gene in pancreatic cancer. Am J Physiol Gastrointest Liver Physiol 2016;310:G1124–G37.
12. Li CM-C, Gocheva V, Oudin MJ, Bhutkar A, Wang SY, Date SR, et al. Foxa2 and Cdx2 cooperate with Nkx2–1 to inhibit lung adenocarcinoma metastasis. Genes Dev 2015;29:1850–62.
13. Tang Y, Shu G, Yuan X, Jing N, Song J. FOXA2 functions as a suppressor of tumor metastasis by inhibition of epithelial-to-mesenchymal transition in human lung cancers. Cell Res 2011;21:316.
14. Zhu C-P, Wang J, Shi B, Hu P-F, Ning B-F, Zhang Q, et al. The transcription factor FOXA2 suppresses gastric tumorigenesis *in vitro* and *in vivo*. Dig Dis Sci 2015;60:109–17.
15. Zhang Z, Yang C, Gao W, Chen T, Qian T, Hu J, et al. FOXA2 attenuates the epithelial to mesenchymal transition by regulating the transcription of E-cadherin and ZEB2 in human breast cancer. Cancer Lett 2015;361:240–50.
16. Perez-Balaguer A, Ortiz-Martínez F, García-Martínez A, Pomares-Navarro C, Lerma E, Peiró G. FOXA2 mRNA expression is associated with relapse in patients with triple-negative/basal-like breast carcinoma. Breast Cancer Res Treat 2015;153:465–74.
17. Li Z, Tuteja G, Schug J, Kaestner KH. Foxa1 and Foxa2 are essential for sexual dimorphism in liver cancer. Cell 2012;148:72–83.
18. Wight TN. Provisional matrix: a role for versican and hyaluronan. Matrix Biol 2017;60–61:38–56.
19. Ghosh S, Albitar L, LeBaron R, Welch WR, Samimi G, Birrer MJ, et al. Up-regulation of stromal versican expression in advanced stage serous ovarian cancer. Gynecol Oncol 2010;119:114–20.
20. Yeung T-L, Leung CS, Wong K-K, Samimi G, Thompson MS, Liu J, et al. TGF-β modulates ovarian cancer invasion by upregulating CAF-derived versican in the tumor microenvironment. Cancer Res 2013;73: 5016–28.
21. Bernaudo S, Salem M, Qi X, Zhou W, Zhang C, Yang W, et al. Cyclin G2 inhibits epithelial-to-mesenchymal transition by disrupting Wnt/β-catenin signaling. Oncogene 2016;35:4816.
22. Ye G, Fu G, Cui S, Zhao S, Bernaudo S, Bai Y, et al. MicroRNA 376c enhances ovarian cancer cell survival by targeting activin receptor-like kinase 7: implications for chemoresistance. J Cell Sci 2011;124:359–68.
23. Fu G, Ye G, Nadeem L, Ji L, Manchanda T, Wang Y, et al. MicroRNA-376c impairs transforming growth factor-beta and nodal signaling to promote trophoblast cell proliferation and invasion. Hypertension 2013; 61:864–72.
24. O'Brien J, Hayder H, Peng C. Automated quantification and analysis of cell counting procedures using ImageJ plugins. J Vis Exp 2016;117:e54719.
25. Fu G, Peng C. Nodal enhances the activity of FoxO3a and its synergistic interaction with Smads to regulate cyclin G2 transcription in ovarian cancer cells. Oncogene 2011;30:3953–66.
26. Pundir S, Martin MJ, O'Donovan C. UniProt Protein Knowledgebase. Methods Mol Biol 2017;1558:41–55.
27. Kent WJ, Sugnet CW, Furey TS, Roskin KM, Pringle TH, Zahler AM, et al. The human genome browser at UCSC. Genome Res 2002;12:996–1006.
28. Sanjana NE, Shalem O, Zhang F. Improved vectors and genome-wide libraries for CRISPR screening. Nat Methods 2014;11:783–4.
29. Gao J, Aksoy B, Dogrusoz U, Dresdner G, Gross B, Sumer S, et al. Integrative analysis of complex cancer genomics and clinical profiles using the cBioPortal. Sci Signal 2013;6:1–20.
30. Metzakopian E, Lin W, Salmon-Divon M, Dvinge H, Andersson E, Ericson J, et al. Genome-wide characterization of Foxa2 targets reveals upregulation of floor plate genes and repression of ventrolateral genes in midbrain dopaminergic progenitors. Development 2012;139:2625–34.
31. Adorno M, Cordenonsi M, Montagner M, Dupont S, Wong C, Hann B, et al. A Mutant-p53/Smad complex opposes p63 to empower TGFbeta-induced metastasis. Cell 2009;137:87–98.
32. Feng Z, Xu X, Cen D, Luo C, Wu S. miR-590-3p promotes colon cancer cell proliferation via Wnt/β-catenin signaling pathway by inhibiting WIF1 and DKK1. Eur Rev Med Pharmacol Sci 2017;21:4844–52.
33. Chen L, Wang W, Zhu S, Jin X, Wang J, Zhu J, et al. MicroRNA-590-3p enhances the radioresistance in glioblastoma cells by targeting LRIG1. Exp Ther Med 2017;14:1818–24.
34. Ge X, Gong L. MiR-590-3p suppresses hepatocellular carcinoma growth by targeting TEAD1. Tumour Biol 2017;39:1010428317695947.
35. Mo M, Peng F, Wang L, Peng L, Lan G, Yu S. Roles of mitochondrial transcription factor A and microRNA-590-3p in the development of bladder cancer. Oncol Lett 2013;6:617–23.
36. Schwede M, Spentzos D, Bentink S, Hofmann O, Haibe-Kains B, Harrington D, et al. Stem cell-like gene expression in ovarian cancer predicts type II subtype and prognosis. PLoS One 2013;8:e57799.
37. Desjardins M, Xie J, Gurler H, Muralidhar GG, Sacks JD, Burdette JE, et al. Versican regulates metastasis of epithelial ovarian carcinoma cells and spheroids. J Ovarian Res 2014;7:70.
38. Sheng W, Wang G, Wang Y, Liang J, Wen J, Zheng PS, et al. The roles of versican V1 and V2 isoforms in cell proliferation and apoptosis. Mol Biol Cell 2005;16:1330–40.

39. Du WW, Yang W, Yee AJ. Roles of versican in cancer biology–tumorigenesis, progression and metastasis. Histol Histopathol 2013;28:701–13.
40. Foulcer SJ, Nelson CM, Quintero MV, Kuberan B, Larkin J, Dours-Zimmermann MT, et al. Determinants of versican-V1 proteoglycan processing by the metalloproteinase ADAMTS5. J Biol Chem 2014;289:27859–73.
41. Committee on the State of the Science in Ovarian Cancer Research, Board on Health Care Services, Institute of Medicine, National Academies of Sciences, Engineering, and Medicine. Ovarian cancers: evolving paradigms in research and care. Washington, DC: National Academies Press; 2016.
42. Kim CW, Oh ET, Kim JM, Park JS, Lee DH, Lee JS, et al. Hypoxia-induced microRNA-590–5p promotes colorectal cancer progression by modulating matrix metalloproteinase activity. Cancer Lett 2018;416:31–41.
43. Yu D, Wolf JK, Scanlon M, Price JE, Hung MC. Enhanced c-erbB-2/neu expression in human ovarian cancer cells correlates with more severe malignancy that can be suppressed by E1A. Cancer Res 1993;53:891–8.
44. Li B, Jin H, Yu Y, Gu C, Zhou X, Zhao N, et al. HOXA10 is overexpressed in human ovarian clear cell adenocarcinoma and correlates with poor survival. Int J Gynecol Cancer 2009;19:1347–52.
45. Domcke S, Sinha R, Levine DA, Sander C, Schultz N. Evaluating cell lines as tumour models by comparison of genomic profiles. Nat Commun 2013;4:2126.
46. Lengyel E, Burdette JE, Kenny HA, Matei D, Pilrose J, Haluska P, et al. Epithelial ovarian cancer experimental models. Oncogene 2014;33:3619–33.

Published OnlineFirst May 10, 2018; DOI: 10.1158/0008-5472.CAN-17-3014

Cancer Research
The Journal of Cancer Research (1916–1930) | The American Journal of Cancer (1931–1940)

AACR American Association for Cancer Research

miR-590-3p Promotes Ovarian Cancer Growth and Metastasis via a Novel FOXA2–Versican Pathway

Mohamed Salem, Jacob A. O'Brien, Stefanie Bernaudo, et al.

Cancer Res 2018;78:4175-4190. Published OnlineFirst May 10, 2018.